

Research Article

Stability of the Shallow Axisymmetric Parabolic-Conic Bimetallic Shell by Nonlinear Theory

M. Jakomin¹ and F. Kosel²

¹ Faculty of Maritime Studies and Transport, University of Ljubljana, Pot Pomorščakov 4, 6320 Portorož, Slovenia

² Faculty of Mechanical Engineering, University of Ljubljana, Aškerčeva 6, 1000 Ljubljana, Slovenia

Correspondence should be addressed to M. Jakomin, marko.jakomin@fpp.edu

Received 13 July 2010; Revised 16 February 2011; Accepted 30 May 2011

Academic Editor: Mohammad Younis

Copyright © 2011 M. Jakomin and F. Kosel. This is an open access article distributed under the Creative Commons Attribution License, which permits unrestricted use, distribution, and reproduction in any medium, provided the original work is properly cited.

In this contribution, we discuss the stress, deformation, and snap-through conditions of thin, axisymmetric, shallow bimetallic shells of so-called parabolic-conic and plate-parabolic type shells loaded by thermal loading. According to the theory of the third order that takes into account the balance of forces on a deformed body, we present a model with a mathematical description of the system geometry, displacements, stress, and thermoelastic deformations. The equations are based on the large displacements theory. We numerically calculate the deformation curve and the snap-through temperature using the fourth-order Runge-Kutta method and a nonlinear shooting method. We show how the temperature of both snap-through depends on the point where one type of the rotational curve transforms into another.

1. Introduction

The development of machine sciences in recent centuries has led to the manufacture of various devices from relatively simple mechanisms to the very complex mechanical devices used by mankind in the process of transforming material goods. Although modern equipment comes in very different forms, functions, and structure, owing to the importance of smooth, reliable operation and their value, a demand for protection against a number of overloads is expressed. It is especially necessary to provide reliable protection against thermal overload for machines that convert one form of energy into another and heat up in the process. For this purpose, elements are built into devices to serve as a “thermal fuse” turning the machine off as soon as an individual part reaches the maximum permissible temperature. Due to their operational reliability, both line and plane bimetallic structural elements are used in protection against thermal overload, whose operation is based on the known physical

fact that bodies expand with the increase of temperature. With a suitable technical act, we can connect a bimetallic construction element, Figure 1, with electrical contacts and make a so-called “thermal switch”. Displacements created on the bimetallic element due to a combination of temperature and mechanical loads turn the device on and off dependent on the temperature T . For this, it is of course necessary to know the connection between the displacements and loading of the bimetallic construction element. Apart from material properties, this connection is also dependent on the geometric properties of the bimetal, as the line bimetallic construction elements respond with different stresses and deformational states to temperature loads as compared to plane construction elements. In practice, the difference in the stability conditions is the most important. Thin and shallow bimetallic shells with suitable material and geometric properties have the characteristic of snapping-through into a new equilibrium position at a certain temperature. The result of such a fast snap-through of a bimetallic shell acting as a switching element in a thermal switch is the instantaneous shutdown of electric power and the machine. The snap-through of the bimetallic shell is a dynamic occurrence that lasts a very short time and as such prevents the damaging sparking and melting of electric contacts and extends the life expectancy of the thermal switch.

Panov, Timoshenko, Videgren, Wittrick, Aggarwala, Saibel, Huai, Vasudevan, Johnson, Keller, Reiss, Brodland, Cohen, Kosel, Batista, Drole, Jakomin, and some other authors have engaged in the research of bimetallic shell elements in a homogenous temperature field. S. Timoshenko [1] researched the problem of the stability of bimetallic lines and plates. The authors Panov [2] and Wittrick et al. [3] researched the problem of the stability for shallow axi-rotational symmetric spherical shells during heating. The related problem of stability of a spherical shell under normal loads has been treated by Keller and Reiss [4]. The problem of thermal stability of a multimetallic strip has been treated by Vasudevan and Johnson in [5]. Aggarwala and Saibel researched the thermal stability of thin spherical shells [6]. The occurrence of the snap-through of an open bimetallic shell was treated by Ren Huai [7] using approximative methods. The problem of finite axisymmetric deflection and snapping of spherical shells which are point loaded at the apex and simply supported at the boundary is analysed by Brodland and Cohen, in [8]. Kosel et al. researched the stability conditions during the temperature and mechanical loading of rotational axisymmetric [9–12] and translation shells [13, 14] with and without an opening at the apex of the shell.

Apart from the spherical and parabolic bimetallic shells, the market also offers shells with more complex initial geometries. “Elektronik Werkstatte” the manufacturer of bimetallic shells from Eichgraben in Austria offers several different types of combined axisymmetric shells (Figure 1, the first and the second shell from the left in the top row) that have an advantage over spherical shells in that the temperature range of the snap-through (the difference in temperature of the upper and lower snap-through) can be changed at the constant of the initial bimetallic shell height. Even with a relatively small initial shell height, using a suitable combination of a parabola and cone rotational curve, it is possible to achieve snap-through of the shell only at very high temperature loads. Due to the smaller initial height, it is important that the stresses in these shells are smaller relative to the stresses in parabolic or spherical shells.

So, this time, we are discussing the stability and deformation conditions for a thin axisymmetric shallow bimetallic shell, composed of a parabola and cone and a plane and parabola. Apart from the temperature, the shell is additionally burdened with a force at the apex and with pressure. When executing a nonlinear mathematical model for the snap-through of a bimetallic translation shell, we will assume a small strain and the moderate rotation of the shell element. In the strain tensor, we will also consider nonlinear terms, while

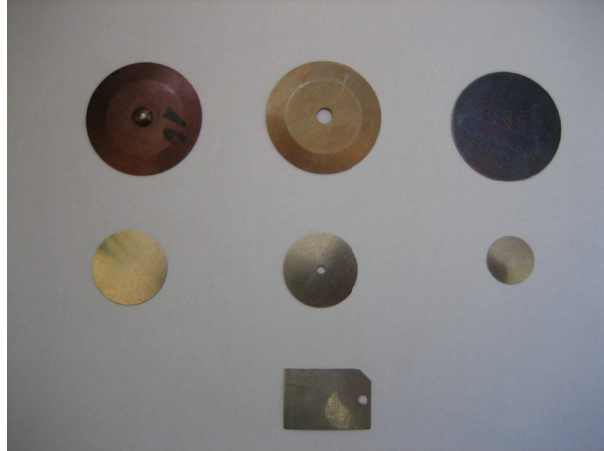


Figure 1: Some of the different types of bimetallic shells made by the Austrian manufacturer “Elektronik Werkstatte”.

placing equilibrium equations on the deformed part of the shell. For the first time, we will show in both table and graphic form how the temperature of both snap-through depends on the point where the parabolic shape of the rotational curve changes into a cone shape. We will explain the effect of the concentrated force at the apex for the example of a bimetallic shell of the plate-parabola type!

The defined thermoelastic problem will be solved with the following steps:

- (1) defining the geometry of the undeformed shell,
- (2) deriving the displacement vector as relation between the geometry of the undeformed and the deformed shell,
- (3) defining the geometry of the deformed shell,
- (4) deriving the elements of the strain and stress tensor,
- (5) introducing the forces and moments per unit of length,
- (6) deriving the equilibrium equations of unit forces and moments acting in the deformed shell element, and
- (7) calculating the deformation curve and the snap-through temperature using the fourth-order Runge-Kutta method and a nonlinear shooting method.

2. Geometry of the Undeformed Shell

The axisymmetric shape of the undeformed shell is formed by rotation of the curve $y = y(x)$, about the y axis [15], Figure 2. The middle surface of the undeformed axisymmetric shell in the Lagrange Coordinate System is, therefore, defined by the function $y = y(x)$. Figure 3 shows the middle surface of a thin rotationally symmetric bimetallic shell.

From Figures 2 and 3, we can obtain the geometric properties of the undeformed shell. Differential of the length in the meridian direction ds_ψ :

$$ds_\psi = r_\psi d\psi. \quad (2.1)$$

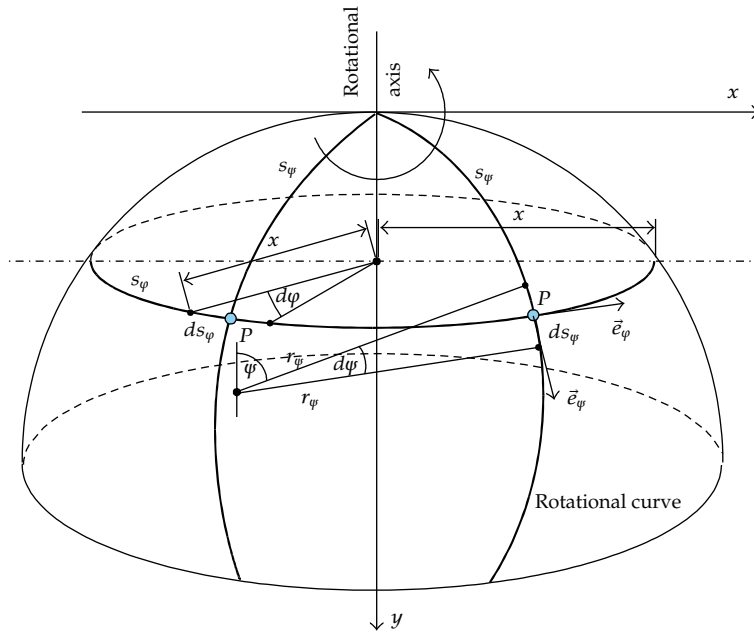


Figure 2: Geometry of the undeformed shell and basis unit vectors.

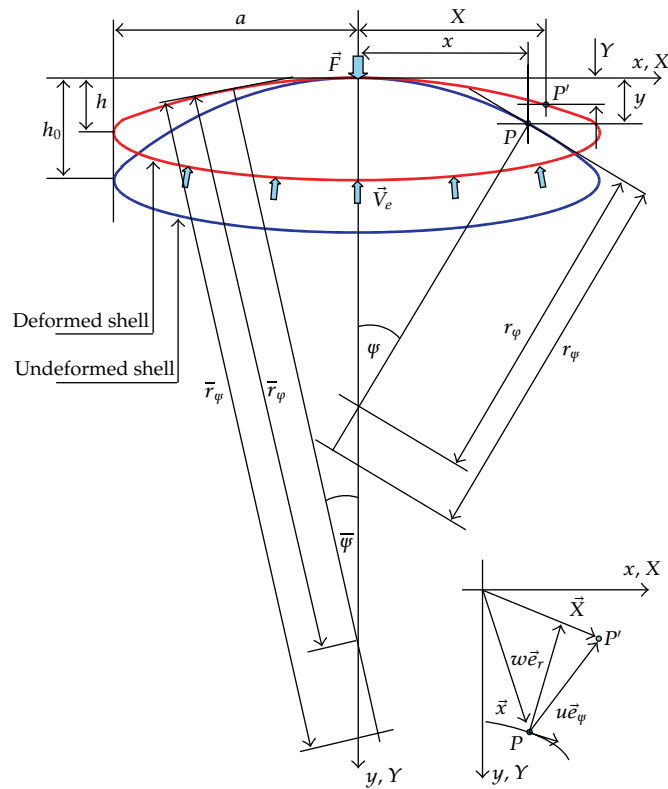


Figure 3: The axisymmetric shell in a homogeneous temperature field and the connection between the Euler and Lagrange coordinate system.

Differential of the length in the circular direction ds_φ is

$$ds_\varphi = r_\varphi \sin \psi \quad d\varphi = x d\psi. \quad (2.2)$$

Meridian angle ψ

$$\psi = \arctan\left(\frac{dy}{dx}\right) = \arctan(y') \approx y'. \quad (2.3)$$

The flexion curvature $1/r_\varphi$ of the rotational curve $y(x)$ in the meridian direction is, Figures 2 and 3

$$\frac{1}{r_\varphi} = \frac{y''}{\sqrt{(1+y'^2)^3}} \approx y''. \quad (2.4)$$

The flexion curvature $1/r_\varphi$ of the circle formed by rotation of the curve $y = y(x)$, in the circular direction is, Figures 2 and 3,

$$\frac{1}{r_\varphi} = \frac{\sin \psi}{x} = \frac{\sin \arctan(y')}{x} = \frac{1}{x} \frac{y'}{\sqrt{1+(y')^2}} \approx \frac{y'}{x}. \quad (2.5)$$

The simplifications in (2.3), (2.4), and (2.5) are justified since we are discussing a shallow shell, where,

$$y'(x)^2 \ll 1, \quad (2.6)$$

and consequently,

$$\sin \psi \approx \psi, \quad \sin \varphi \approx \varphi, \quad \cos \psi \approx 1. \quad (2.7)$$

3. Displacement Vector and Geometry of Deformed Shell

Due to the temperature change, the shell deforms into a new shape defined by the function $Y(X)$ in the Euler Coordinate System. Since we are discussing a thin double-layered shell, the displacement field is selected to satisfy the Kirchhoff hypothesis [16]:

- (1) straight lines perpendicular to the shell's middle surface before deformation, remain straight after deformation,
- (2) the transverse normals do not experience elongation,
- (3) the transverse normals rotate, so that they remain perpendicular to the shell's middle surface after deformation.

The reader should note that the Kirchhoff hypothesis stating that the thickness of the shell before and after deformation remains the same when the shell is subjected to kinematic

constraint is not realistic when large strains are admitted in the deformation process [17]. The so-called Zig-Zag theory is known in literature and describes a piecewise continuous displacement field in the direction of the multilayered shell thickness and accomplishes the continuity of transverse stresses at each layer [18–20]. However, given the fact that the ratio between the thickness and length of bimetallic shells, used as safety constructional elements against temperature overheating, is about 1/100, we found the Kirchhoff hypothesis is fully acceptable for our mathematical model.

The new shape of the shell in a deformed state is axisymmetric due to the homogeneous temperature field and axisymmetric mechanical load. Therefore, the displacement v in the circular direction as well as other shell properties relative to the angle φ do not change:

$$v = 0, \quad \frac{\partial}{\partial \varphi} (\) = 0. \quad (3.1)$$

The displacement vector \vec{u} of any point P on the middle surface of an undeformed shell defines the point P' on the middle surface of a deformed shell

$$\vec{u} = u\vec{e}_\varphi + v\vec{e}_\varphi + w\vec{e}_r, \quad (3.2)$$

and with the supposition (3.1),

$$\vec{u} = u\vec{e}_\varphi + w\vec{e}_r. \quad (3.3)$$

Unit basis vectors \vec{e}_φ , \vec{e}_φ and \vec{e}_r in the Cartesian coordinate system follow directly from the system geometry, Figure 2,

$$\begin{aligned} \vec{e}_\varphi &= (\cos \psi \cos \varphi)\vec{i} + (\sin \psi)\vec{j} + (\cos \psi \sin \varphi)\vec{k}, \\ \vec{e}_\varphi &= (-\sin \varphi)\vec{i} + (\cos \varphi)\vec{k}, \\ \vec{e}_r &= (\sin \psi \cos \varphi)\vec{i} - (\cos \psi)\vec{j} + (\sin \psi \sin \varphi)\vec{k}. \end{aligned} \quad (3.4)$$

These vectors are mutually orthogonal because

$$\vec{e}_\varphi \vec{e}_\varphi = \vec{e}_\varphi \vec{e}_r = \vec{e}_\varphi \vec{e}_r = 0. \quad (3.5)$$

Derivatives of these vectors with respect to the curvilinear coordinates ψ , φ , and r are [21]

$$\begin{aligned} \frac{\partial \vec{e}_\varphi}{\partial \psi} &= (-\cos \varphi \sin \psi)\vec{i} + (\cos \psi)\vec{j} - (\sin \psi \sin \varphi)\vec{k} = -\vec{e}_r, \\ \frac{\partial \vec{e}_\varphi}{\partial \varphi} &= (-\cos \psi \sin \varphi)\vec{i} + 0\vec{j} + (\cos \psi \cos \varphi)\vec{k} = \vec{e}_\varphi \cos \psi, \\ \frac{\partial \vec{e}_\varphi}{\partial r} &= \vec{0}, \quad \frac{\partial \vec{e}_\varphi}{\partial \psi} = \vec{0}, \quad \frac{\partial \vec{e}_\varphi}{\partial \varphi} = (-\cos \varphi)\vec{i} + 0\vec{j} + (-\sin \varphi)\vec{k} = -\vec{e}_r \sin \psi - \vec{e}_\varphi \cos \psi, \end{aligned}$$

$$\begin{aligned}\frac{\partial \vec{e}_\varphi}{\partial r} &= \vec{0}, & \frac{\partial \vec{e}_r}{\partial \varphi} &= (\cos \varphi \cos \varphi) \vec{i} + (\sin \varphi) \vec{j} + (\cos \varphi \sin \varphi) \vec{k} = \vec{e}_\varphi, \\ \frac{\partial \vec{e}_r}{\partial \varphi} &= (-\sin \varphi \sin \varphi) \vec{i} + 0 \vec{j} + (\cos \varphi \sin \varphi) \vec{k} = \vec{e}_\varphi \sin \varphi, & \frac{\partial \vec{e}_r}{\partial r} &= \vec{0},\end{aligned}\quad (3.6)$$

and when simplified due to the supposition(2.7)

$$\begin{aligned}\frac{\partial \vec{e}_\varphi}{\partial \varphi} &= -\vec{e}_r, & \frac{\partial \vec{e}_\varphi}{\partial \varphi} &= \vec{e}_\varphi, & \frac{\partial \vec{e}_\varphi}{\partial r} &= \vec{0}, \\ \frac{\partial \vec{e}_\varphi}{\partial \varphi} &= \vec{0}, & \frac{\partial \vec{e}_\varphi}{\partial \varphi} &= -\varphi \vec{e}_r - \vec{e}_\varphi, & \frac{\partial \vec{e}_\varphi}{\partial r} &= \vec{0}, \\ \frac{\partial \vec{e}_r}{\partial \varphi} &= \vec{e}_\varphi, & \frac{\partial \vec{e}_r}{\partial \varphi} &= \varphi \vec{e}_\varphi, & \frac{\partial \vec{e}_r}{\partial r} &= \vec{0}.\end{aligned}\quad (3.7)$$

Now, let us observe displacements on a thin shallow axisymmetric bimetallic shell in a homogenous temperature field, Figure 3, which is additionally loaded with the force \vec{F} at its apex.

The point P at the position $P(x, y(x))$ on the undeformed shell moves into the position P' on the deformed shell with the coordinates $P'(X, Y(X))$. The reader should note that both the Euler $(X, Y(X))$ and Lagrange $(x, y(x))$ coordinate system have the same origin at point $(0, 0)$. So, when a force or temperature load is exerted on the shell the optional point P moves, as we have shown in Figure 3, since the reaction force per unit of length \vec{V}_e acts in the opposite direction. The connection between the Euler $(X, Y(X))$ and Lagrange $(x, y(x))$ Coordinate System is, Figure 3,

$$\vec{X} = \vec{x} + \vec{u}, \quad (3.8)$$

where

$$\vec{u}(x, y) = \begin{bmatrix} \cos \varphi & \sin \varphi \\ \sin \varphi & -\cos \varphi \end{bmatrix} \begin{bmatrix} u \\ w \end{bmatrix}, \quad (3.9)$$

from which we obtain

$$X = x + w \sin \varphi + u \cos \varphi \approx x + w y' + u, \quad (3.10)$$

$$Y = y - w \cos \varphi + u \sin \varphi \approx y - w. \quad (3.11)$$

In (3.10), we also consider that the displacement u is small in comparison with the displacement w , which in turn is small in comparison with the Lagrange coordinates x so

that the Euler coordinates X is approximately

$$X = x + wy' + u \approx x. \quad (3.12)$$

From Figure 3, we can also find geometric properties of the deformed shell.

The differential of the length $d\bar{s}_\psi$ in the meridian direction

$$d\bar{s}_\psi = \bar{r}_\psi d\bar{\psi} = \sqrt{dX^2 + dY^2} = dx\sqrt{X'^2 + Y'^2}. \quad (3.13)$$

Meridian angle $\bar{\psi}$ is

$$\bar{\psi} = \arctan\left(\frac{dY}{dX}\right) \approx \frac{dY}{dX} \approx \frac{dYdx}{dXdX} = \frac{Y'}{X'} \approx Y'. \quad (3.14)$$

Flexion curvature $1/\bar{r}_\psi$ in the meridian direction is

$$\frac{1}{\bar{r}_\psi} = \frac{\left| \frac{X'}{X''} \frac{Y'}{Y''} \right|}{\sqrt{(X'^2 + Y'^2)^3}} \cong Y''. \quad (3.15)$$

Flexion curvature $1/\bar{r}_\varphi$ in the circular direction

$$\frac{1}{\bar{r}_\varphi} = \frac{\sin \bar{\psi}}{X} \approx \frac{\bar{\psi}}{X} \cong \frac{dY}{dX} \frac{1}{X} \cong \frac{Y'}{X}. \quad (3.16)$$

With (3.11) and (3.12) for Euler's coordinates Y and X , we finally obtain

$$\bar{\psi} = y' - w', \quad \frac{1}{\bar{r}_\psi} = y'' - w'', \quad \frac{1}{\bar{r}_\varphi} = \frac{y' - w'}{x}. \quad (3.17)$$

4. Strain and Stress Tensor

A shell's deformation state is shown by the displacement vector \vec{u} in the middle, that is, reference surface. This vector has two components: the displacement u in the meridian direction and the displacement w in the radial direction. The elements of the strain tensor \mathbf{E} in the curvilinear orthogonal coordinate system are determined by the Green-Lagrange strain tensor \mathbf{E} for the middle surface of the shell [16]

$$\mathbf{E} = \mathbf{E}^T = \frac{1}{2} \left[\vec{\nabla} \otimes \vec{u} + (\vec{\nabla} \otimes \vec{u})^T + (\vec{\nabla} \otimes \vec{u}) \cdot (\vec{\nabla} \otimes \vec{u})^T \right], \quad (4.1)$$

where the displacement vector \vec{u} is of the form (3.3). The vector operator $\vec{\nabla}$ is by definition

$$\vec{\nabla} = \vec{e}_\psi \frac{\partial}{\partial s_\psi} + \vec{e}_\varphi \frac{\partial}{\partial s_\varphi} + \vec{e}_r \frac{\partial}{\partial z} = \vec{e}_\psi \frac{1}{r_\psi} \frac{\partial}{\partial \psi} + \vec{e}_\varphi \frac{1}{x} \frac{\partial}{\partial \varphi} + \vec{e}_r \frac{\partial}{\partial z}. \quad (4.2)$$

The gradient of the displacement vector \vec{u} , while keeping in mind the derivatives of the unit basis vectors (3.7) and supposition (3.1), in the Green-Lagrange strain tensor (4.1) is

$$\text{grad } \vec{u} = \vec{\nabla} \otimes \vec{u} = \begin{pmatrix} p_{11} & p_{12} & p_{13} \\ p_{21} & p_{22} & p_{23} \\ p_{31} & p_{32} & p_{33} \end{pmatrix} = \begin{pmatrix} \frac{1}{r_\psi} \left(\frac{\partial u}{\partial \psi} + w \right), & 0, & \frac{1}{r_\psi} \left(\frac{\partial w}{\partial \psi} - u \right) \\ 0, & \frac{1}{r_\psi \psi} (u + w\psi), & 0 \\ \frac{\partial u}{\partial z'}, & 0, & \frac{\partial w}{\partial z} \end{pmatrix}. \quad (4.3)$$

All nine tensor elements are obtained once (4.3) is inserted into (4.1):

$$\mathbf{E} = \frac{1}{2} \begin{pmatrix} 2p_{11} + p_{11}^2 + p_{12}^2 + p_{13}^2, & p_{12} + p_{21} + p_{11} p_{21} + p_{12} p_{22} + p_{13} p_{23}, & p_{13} + p_{31} + p_{11} p_{31} + p_{12} p_{32} + p_{13} p_{33} \\ p_{12} + p_{21} + p_{11} p_{21} + p_{12} p_{22} + p_{13} p_{23}, & 2p_{22} + p_{21}^2 + p_{22}^2 + p_{23}^2, & p_{23} + p_{32} + p_{21} p_{31} + p_{22} p_{32} + p_{23} p_{33} \\ p_{13} + p_{31} + p_{11} p_{31} + p_{12} p_{32} + p_{13} p_{33}, & p_{23} + p_{32} + p_{21} p_{31} + p_{22} p_{32} + p_{23} p_{33}, & 2p_{33} + p_{31}^2 + p_{32}^2 + p_{33}^2 \end{pmatrix}, \quad (4.4)$$

or in explicit form

$$\begin{aligned} \varepsilon_\psi &= \frac{1}{r_\psi} \left(\frac{\partial u}{\partial \psi} + w \right) + \frac{1}{2r_\psi^2} \left(u^2 + w^2 + 2w \frac{\partial u}{\partial \psi} - 2u \frac{\partial w}{\partial \psi} + \left(\frac{\partial u}{\partial \psi} \right)^2 + \left(\frac{\partial w}{\partial \psi} \right)^2 \right), \\ \varepsilon_\varphi &= \frac{1}{r_\varphi} \left(\frac{1}{\psi} u + w \right) + \frac{1}{2r_\varphi^2} \left(w^2 + \frac{2u w}{\psi} + \frac{1}{\psi^2} (u^2 + v^2) \right), \\ \varepsilon_{\psi r} = \varepsilon_{r\psi} &= \frac{1}{2} \frac{\partial u}{\partial z} + \frac{1}{2r_\psi} \left(\frac{\partial w}{\partial \psi} - u \right) + \frac{1}{2r_\psi} \left(w \frac{\partial u}{\partial z} - u \frac{\partial w}{\partial z} + \frac{\partial u}{\partial z} \frac{\partial u}{\partial \psi} + \frac{\partial w}{\partial z} \frac{\partial w}{\partial \psi} \right), \\ \varepsilon_{rr} &= \frac{\partial w}{\partial z} + \frac{1}{2} \left(\left(\frac{\partial u}{\partial z} \right)^2 + \left(\frac{\partial w}{\partial z} \right)^2 \right), \\ \varepsilon_{\psi\psi} &= 0, \quad \varepsilon_{\varphi\varphi} = 0, \quad \varepsilon_{\varphi r} = \varepsilon_{r\varphi} = 0. \end{aligned} \quad (4.5)$$

However, the strains in (4.4) and (4.5) are still cumbersome and can hardly be used in practical computation. On the other hand, some nonlinear terms are relatively small and can be neglected without any significant effect on the accuracy of the results. Let us find the terms to be neglected.

In the case of rotation ω of the shell element with the length $d\mathbf{s}_\psi$ in the direction of the unit vector \vec{e}_ψ , Figure 4, we can express the differential of the displacement vector $d\vec{u}$ with

$$d\vec{u} = |d\vec{u}| (-\cos \theta \vec{e}_\psi + \sin \theta \vec{e}_r) = d\vec{x} \text{ grad } \vec{u} = ds_\psi (p_{11} \vec{e}_\psi + p_{13} \vec{e}_r), \quad (4.6)$$

where θ is angle that the vector $d\vec{u}$ forms with the basis unit vector \vec{e}_ψ , Figure 4.

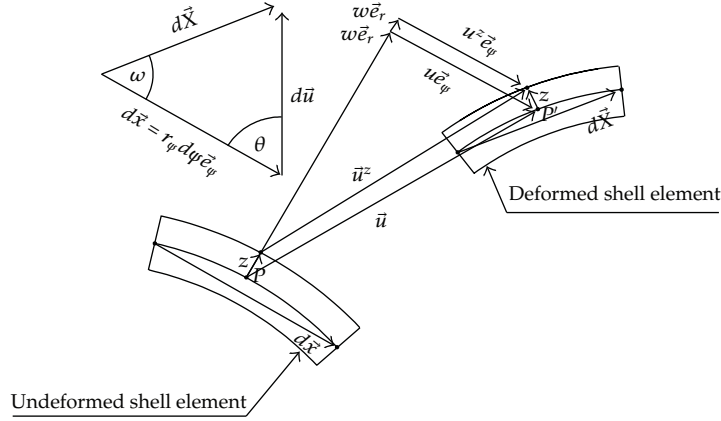


Figure 4: The shell middle surface displacement \vec{u} and displacement \vec{u}^z depending on the local coordinate z as well as the rotation of the shell element ω .

In the case of small strains $|\varepsilon_\varphi| \ll 1$, we have

$$\begin{aligned} |d\vec{X}| &= |d\vec{x}|(1 + \varepsilon_\varphi) \approx |d\vec{x}|, \\ |d\vec{u}| &\approx |d\vec{x}|\omega \approx r_\varphi d\psi \omega = ds_\varphi \omega, \end{aligned} \quad (4.7)$$

where ω as the rotation of the shell element is expressed in radians. It is also further evident by comparing the coefficients in (4.6) that

$$p_{11} = -\frac{|d\vec{u}|}{ds_\varphi} \cos \theta = -\omega \cos \theta \quad p_{13} = \frac{|d\vec{u}|}{|d\psi|} \sin \theta = \omega \sin \theta. \quad (4.8)$$

If the shell element with the length ds_φ in the direction of the unit vector \vec{e}_φ completes the rotation for the angle $\omega = 20^\circ$ around the vector \vec{e}_φ , it follows that:

$$p_{11} \approx \frac{-\pi}{9} \cos 80^\circ \approx -0.06 \quad p_{13} \approx \frac{\pi}{9} \sin 80^\circ \approx 0.34. \quad (4.9)$$

A similar calculation can be performed for the rotation of the shell element with the length ds_φ in the direction of the unit vector \vec{e}_φ .

In case of small strains and moderate shell rotations approximately up to 20° , the components of the displacement gradient are

$$\{|p_{11}|, |p_{22}|, |p_{33}|\} \ll 1, \quad (4.10)$$

$$\{|p_{13}|\} < 1, \quad (4.11)$$

due to which we ignore all nonlinear terms in Green-Lagrange strain tensor (4.4) except the term p_{13}^2 .

Thus, the displacement of the point P due to load is the largest in the direction of the unit vector \vec{e}_r , while the displacement in the direction of the unit vectors \vec{e}_ψ is by absolute value smaller

$$|u| < |\omega|. \quad (4.12)$$

Further, we consider that the flexion curvature of the shallow shell in the meridian direction is very small due to which it is true that

$$\frac{1}{r_\psi} u \approx y'' u \ll \frac{1}{r_\psi} \frac{d\omega}{d\psi} = \frac{d\omega}{ds_\psi} \approx \frac{d\omega}{dx} = \omega'. \quad (4.13)$$

So, the tensor elements (4.4) and (4.5) are finally

$$\mathbf{E} = \frac{1}{2} \begin{pmatrix} 2p_{11} + p_{13}^2 & 0 & p_{13} + p_{31} \\ 0 & 2p_{22} & 0 \\ p_{13} + p_{31} & 0 & 2p_{33} \end{pmatrix}, \quad (4.14)$$

or

$$\begin{aligned} \varepsilon_\psi &= \frac{1}{r_\psi} \left(\frac{\partial u}{\partial \psi} + \omega \right) + \frac{1}{2r_\psi^2} \left(\frac{\partial \omega}{\partial \psi} \right)^2, & \varepsilon_\varphi &= \frac{1}{r_\varphi} \left(\frac{1}{\psi} u + \omega \right), \\ \varepsilon_{\psi r} = \varepsilon_{r\psi} &= \frac{1}{2} \frac{\partial u}{\partial z} + \frac{1}{2r_\psi} \frac{\partial \omega}{\partial \psi}, & \varepsilon_{r\psi} &= \frac{\partial \omega}{\partial z}, \\ \varepsilon_{\psi\psi} &= 0, & \varepsilon_{\varphi\varphi} &= 0, & \varepsilon_{\varphi r} = \varepsilon_{r\varphi} &= 0. \end{aligned} \quad (4.15)$$

With the introduction of the local coordinate z with the centre of origin on the middle surface of the shell, Figure 4, the elements of the strain tensor \mathbf{E} are, due to the shell's curvature, also the function of the coordinate z . The relation between the displacement u^z on the local coordinate z and displacement u on the middle surface of the bimetallic shell, Figure 4, can be found from the strain tensor element $\varepsilon_{\psi r}$, since Kirchhoff hypothesis states that the strain lines perpendicular to the shell's middle surface before deformation remain straight also after deformation. In other words, the hypothesis declares that the shear strain $\varepsilon_{\psi r}$ is zero

$$\varepsilon_{\psi r} = \frac{1}{2} \frac{\partial u}{\partial z} + \frac{1}{2r_\psi} \frac{\partial \omega}{\partial \psi} = 0. \quad (4.16)$$

The solution to this equation with respect to the element u of the displacement vector \vec{u} is:

$$u(z) = u^z = u - \frac{z}{r_\psi} \frac{\partial \omega}{\partial \psi}. \quad (4.17)$$

The normal strain ε_r in the transversal direction is equal to zero according to the second assumption of Kirchhoff's hypothesis:

$$\varepsilon_r = 0. \quad (4.18)$$

Now, two nonzero elements of the Green-Lagrange strain tensor \mathbf{E} (4.15) for the middle surface of the shell can be recorded by means of relation (4.13) as

$$\begin{aligned} \varepsilon_\psi &= u' + \omega y'' + \frac{1}{2}(\omega')^2, \\ \varepsilon_\varphi &= \frac{u + y'\omega}{x}. \end{aligned} \quad (4.19)$$

Note again that when we form the strain tensor \mathbf{E} , we retain the nonlinear term for strain ε_ψ in u^z the meridian direction according to the third order of the large displacements theory. Namely, it has been confirmed that taking into account this nonlinear term is crucial for the accuracy of the results.

We calculate the strains ε_ψ^z and ε_φ^z at distance z from the middle surface of the bimetallic shell in the direction of the unit vector \vec{e}_r with (4.15), where we replace the displacement u with the displacement u^z .

Since we are working on a thin shell, where $z \ll \{r_\psi, r_\varphi\}$, we obtain

$$\begin{aligned} \varepsilon_\psi^z &= (u^z)' + \frac{\omega}{r_\psi + z} + \frac{1}{2}(\omega')^2 = (u - z\omega')' + \frac{\omega}{r_\psi + z} + \frac{1}{2}(\omega')^2 \approx \varepsilon_\psi - z\omega'', \\ \varepsilon_\varphi^z &= \frac{1}{r_\varphi + z} \left(\frac{u^z}{\psi} + \omega \right) = \frac{1}{r_\varphi + z} \left(\frac{u - z\omega'}{\psi} + \omega \right) \approx \varepsilon_\varphi - \frac{z\omega'}{x}. \end{aligned} \quad (4.20)$$

The relation between the strain and stress tensor is determined by Hooke's law [22]

$$\begin{aligned} \sigma_\psi^z &= \frac{E}{1 - \mu^2} \left(\mu \varepsilon_\psi^z + \varepsilon_\psi^z - (1 + \mu)\alpha T \right), \\ \sigma_\varphi^z &= \frac{E}{1 - \mu^2} \left(\mu \varepsilon_\varphi^z + \varepsilon_\varphi^z - (1 + \mu)\alpha T \right). \end{aligned} \quad (4.21)$$

The symbol E denotes the Young's modulus, the symbol μ denotes the Poisson's ratio and α is the thermal expansion coefficient. The symbol T denotes the shell's relative temperature relevant to the reference T_0 for which the stress state in the shell is equal to zero:

$$\sigma_\psi^z(x, z, T_0) = \sigma_\varphi^z(x, z, T_0) = \tau_{\psi r}^z(x, z, T_0) = 0. \quad (4.22)$$

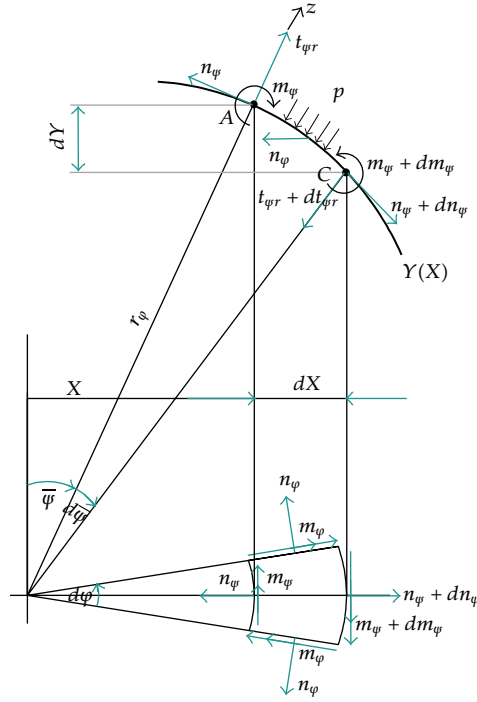


Figure 6: Unit forces and moments in the element of a deformed shell and external pressure load p .

In doing so, let us also remember that we are discussing a shallow shell, where the sinus function of the meridian angle $\bar{\psi}$ can be replaced by its argument $\bar{\psi}$, while the cosine of the same angle is very close to one

$$\sin \bar{\psi} \approx \bar{\psi}, \quad \cos \bar{\psi} \approx 1. \quad (5.3)$$

Equilibrium of the forces in the meridian direction is

$$(dN_\varphi + d(dN_\varphi)) - dN_\varphi - dT_{\varphi r} d\bar{\psi} + p\bar{r}_\varphi d\bar{\psi} X d\varphi \frac{d\bar{\psi}}{2} - dN_\varphi d\varphi = 0. \quad (5.4)$$

Equilibrium of the forces in the radial direction

$$(dT_{\varphi r} + d(dT_{\varphi r})) - dT_{\varphi r} + p\bar{r}_\varphi d\bar{\psi} X d\varphi + dN_\varphi d\bar{\psi} + dN_\varphi d\varphi \left(\bar{\psi} + \frac{d\bar{\psi}}{2} \right) = 0. \quad (5.5)$$

The equilibrium equation of forces in the circular direction cannot be considered due to the axisymmetric deformation. We write the moment equilibrium as

$$\begin{aligned}
& (dM_\varphi + d(dM_\varphi)) - dM_\varphi - 2dM_\varphi \left(\frac{d\varphi}{2} \right) - dT_{\varphi r} dX - dT_{\varphi r} \bar{\varphi} dY \\
& + p\bar{r}_\varphi d\bar{\varphi} X d\varphi \left(\frac{dX}{2} + \left(\bar{\varphi} + \frac{d\bar{\varphi}}{2} \right) \frac{dY}{2} \right) \\
& - dN_\varphi \bar{\varphi} dX + dN_\varphi dY + 2dN_\varphi \frac{d\varphi}{2} \frac{dY}{2} = 0,
\end{aligned} \tag{5.6}$$

where

$$\begin{aligned}
d(dN_\varphi) &= \frac{\partial(dN_\varphi)}{\partial\varphi} d\varphi = dn_\varphi X d\varphi + n_\varphi dX d\varphi, \\
d(dT_{\varphi r}) &= \frac{\partial(dT_{\varphi r})}{\partial\varphi} d\varphi = dt_{\varphi r} X d\varphi + t_{\varphi r} dX d\varphi, \\
d(dM_\varphi) &= \frac{\partial(dM_\varphi)}{\partial\varphi} d\varphi = dm_\varphi X d\varphi + m_\varphi dX d\varphi.
\end{aligned} \tag{5.7}$$

After arranging and using (3.17), the equilibrium equations are

$$(n_\varphi x)' - n_\varphi - t_{\varphi r} x (y - w)'' = 0, \tag{5.8}$$

$$(t_{\varphi r} x)' + n_\varphi (y - w)' + n_\varphi x (y - w)'' + px = 0, \tag{5.9}$$

$$(m_\varphi x)' - m_\varphi - t_{\varphi r} x = 0. \tag{5.10}$$

6. Solving Equilibrium Equations

The system of thermoelastic equations for a thin shallow axisymmetric bimetallic shell consists of three equilibrium equations (5.8), (5.9), (5.10), the four equations (5.2) for unit forces and moments, two equations (4.21) for stresses in the shell, two equations (4.20) for strains outside the middle plan of the shell, and finally two equations (4.19) which relate strains and displacements. Thus, the system has 13 equations and as many unknowns, namely n_φ , n_φ , $t_{\varphi r}$, m_φ , m_φ , σ_φ^z , σ_φ^z , ε_φ^z , ε_φ^z , ε_φ , ε_φ , u and w and can be reduced further in a following way: first, we insert (4.20) into (5.2). After integration, we have

$$n_\varphi = A(\varepsilon_\varphi + \mu \varepsilon_\varphi) - PT, \tag{6.1}$$

$$n_\varphi = A(\varepsilon_\varphi + \mu \varepsilon_\varphi) - PT, \tag{6.2}$$

$$m_\psi = B \left(w'' + \mu \frac{w'}{x} \right) - QT, \quad (6.3)$$

$$m_\varphi = B \left(\frac{w'}{x} + \mu w'' \right) - QT, \quad (6.4)$$

where A, B, P , and Q are constants as follows [13, 14]:

$$A = \frac{E\delta}{1-\mu^2}, \quad B = \frac{E\delta^3}{12(1-\mu^2)}, \quad P = \frac{E\delta}{2(1-\mu)}(\alpha_1 + \alpha_2), \quad Q = \frac{E\delta^2(\alpha_2 - \alpha_1)}{8(\mu - 1)}. \quad (6.5)$$

We now multiply (5.8) with $(y' - w')$ and add (5.9). So, we obtain

$$(n_\psi x)'(y - w)' + n_\psi x(y - w)'' + (t_{\psi rr} x)' + px - t_{\psi rr} x(y - w)'(y - w)'' = 0. \quad (6.6)$$

We disregard the last nonlinear term of 10^{-3} magnitude order, since

$$(y' - w')(y'' - w'') = Y'Y'' = \frac{1}{2}(Y'^2)' \approx 10^{-3} \ll 1. \quad (6.7)$$

In this way, we obtain the relation

$$(t_{\psi rr} x)' = -\left(n_\psi x(y - w)'\right)' - px = -\left(n_\psi x(y - w)' + \int px dx\right)', \quad (6.8)$$

and after integration

$$t_{\psi rr} = \frac{1}{x} \left(c - \int_0^x px dx \right) - n_\psi (y - w)', \quad (6.9)$$

where c is a constant that depends exclusively on the external force F acting on the shell.

The relation (6.9) is inserted into (5.9) and (5.10).

$$\begin{aligned} (n_\psi x)' - n_\psi &= 0, \\ (m_\psi x)' - m_\psi + n_\psi x (y - w)' - c + \int_0^x px dx &= 0. \end{aligned} \quad (6.10)$$

We now express the unit forces n_ψ, n_φ and moments m_ψ, m_φ in the equations above with (6.1), (6.2), (6.3), and (6.4), and the strains $\varepsilon_\psi, \varepsilon_\varphi$ with the kinematic equations (4.19). Therefore, the

dependent unknown variables by which we solve the differential equations (6.10) are the elements u and w of the displacement vector \vec{u}

$$u + wy' = x \left(u' + (1 - \mu) \frac{(w')^2}{2} + w'(\mu y' + x(w'' + y'')) + (xu'' + w(y'' + xy''')) \right), \quad (6.11)$$

$$cx + Bw' = x \left(\int_0^x p(x) dx + Bw'' - (w' - y') \right) \times \left(-PTx + A \left(\mu u + \mu wy' + x \left(u' + \frac{(w')^2}{2} + wy'' \right) \right) \right) + Bxw'''. \quad (6.12)$$

We define the integration constant c in (6.12) by taking into account the equilibrium of forces on the edge of the shell.

If a shallow shell is simply supported, the supporting force $t_{\varphi r}$ per unit of length at the edge of the shell is directed opposite to and in value equal to the sum of the force F and pressure p acting on the shell, Figure 7

$$t_{\varphi r} |_{x=a} = -\frac{1}{2\pi a} \left(F + 2\pi \int_0^a p(x) x dx \right), \quad (6.13)$$

equation (6.13) is inserted into (6.9) from where the constant c is expressed

$$c = \frac{-F}{2\pi}. \quad (6.14)$$

If the bimetallic shell serves as a thermal switch shutting down a device in the case of it overheating, then it is necessary to assure that the shell can extend unrestricted in a horizontal direction [10]. In continuation, we will discuss a simply supported shell. At the boundary of the simply supported shell, the force and moment per unit of length are equal to zero

$$n_{\varphi}(a) = n_{\varphi}(-a) = m_{\varphi}(a) = m_{\varphi}(-a) = 0. \quad (6.15)$$

We use (6.1) and (6.3)

$$-PT + A \left(u' + \frac{1}{2} (w')^2 + \frac{\mu(u + wy')}{x} + wy'' \right) \Big|_{x=\pm a} = 0, \quad (6.16)$$

$$-QT + \frac{B\mu w'}{x} + Bw'' \Big|_{x=\pm a} = 0. \quad (6.17)$$

The displacement w at the apex of the shell is equal to zero in the chosen coordinate system:

$$w(0) = 0. \quad (6.18)$$

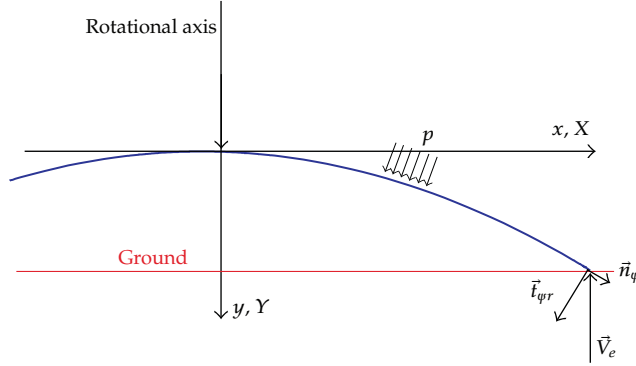


Figure 7: Loading of a simply roller supported shell with the force \vec{F} [N] and external pressure p [N/m²].

It is also demonstrated that this system of (6.11), (6.12), (6.16), (6.17), and (6.18) has symmetry. Namely, if the displacement vector $\vec{u}(x) = u \vec{e}_\psi + w \vec{e}_r$ is the solution to this system, then the solution is also

$$\vec{u}(-x) = -u\vec{e}_\psi + w\vec{e}_r. \quad (6.19)$$

due to which it is sufficient that we solve the system of equations only for positive x values in the interval $[0 \leq x \leq a]$. For negative x , the displacement vector \vec{u} is defined by (6.19). The boundary conditions for the displacement vector \vec{u} also follow from the mentioned symmetry:

$$u(0) = 0, \quad w(0) = 0, \quad w'(0) = 0. \quad (6.20)$$

The remaining conditions on the edges of the shell at $x = a$ are defined with unit forces and moments in the equations for boundary conditions (6.16) and (6.17).

Boundary value problem (BVP) for the snap-through of the system of a shallow axisymmetric bimetallic shell is therefore composed of equilibrium equations (6.11) and (6.12), boundary conditions (6.16) and (6.17) at the point $x = a$, and boundary conditions (6.20) at the point $x = 0$

$$\begin{aligned} u + wy' &= x \left(u' + (1 - \mu) \frac{(w')^2}{2} + w'(\mu y' + x(w'' + y'')) + (xu'' + w(y'' + xy''')) \right), \\ cx + Bw' &= x \left(\int_0^x p x dx + Bw'' - (w' - y') \right. \\ &\quad \left. \times \left(-PTx + A \left(\mu u + \mu wy' + x \left(u' + \frac{(w')^2}{2} + wy'' \right) \right) \right) + Bxw''' \right), \\ PT &= A \left(u' + \frac{1}{2}(w')^2 + \frac{\mu(u + wy')}{x} + wy'' \right) \Big|_{x=a}, \\ QT &= \left(\frac{B\mu w'}{x} + Bw'' \right) \Big|_{x=a}, \quad u(0) = w(0) = w'(0) = 0. \end{aligned} \quad (6.21)$$

7. Analysis of Stability Conditions in a Spherical-Conic Type Bimetallic Shell

In continuation, we will discuss the snap-through and stability conditions during the loading of a parabolic-conic shell composed of a parabola near the apex and of a cone for the rest, Figures 8 and 9, where the rotational curve is determined by the function y

$$y(x) = \begin{cases} kx^2, & x \leq b, \\ k(a+b)x - abk, & x > b, \end{cases} \quad (7.1)$$

with the following material and geometric properties:

$$\begin{aligned} k &= \frac{1}{15^2 \text{ mm}}, & a &= 15 \text{ mm}, & \delta &= 0.3 \text{ mm}, \\ \mu &= \frac{1}{3}, & a_1 &= 3.41 \cdot 10^{-5} \text{ K}, & a_2 &= 1.41 \cdot 10^{-5} \text{ K}. \end{aligned} \quad (7.2)$$

7.1. Analytic Solution in the Case of Flattened Parabolic Shell

The parameter b in the rotational curve function (7.1) defines the point at which the parabola translates into a straight line. If in (7.1) the parameter b is equal to the horizontal radius of the shell a , therefore, $b = a$, we obtain a parabolic shell with the rotational curve $y(x) = kx^2$, Figure 10. Let this parabolic shell be loaded only with the temperature T . Suppose also that the shell at a certain temperature $T = T_m$ is completely flattened, Figure 11. The displacement function $w(x)$ is in that case

$$w(x) = y(x) = kx^2. \quad (7.3)$$

We insert (7.3) into the boundary condition (6.17) and express the temperature T_m at which the shell is flattened

$$T_m = \frac{4k\delta}{3(\alpha_1 - \alpha_2)}. \quad (7.4)$$

With the displacement w as defined by (7.3), the moment equilibrium equation (6.12) is identically satisfied

$$\begin{aligned} & Bw' - x \left(Bw'' - (w' - y') \left(-PTx + A \left(\mu u + \mu w y' + x \left(u' + \frac{(w')^2}{2} + w y'' \right) \right) \right) \right) + Bxw''' \\ & \equiv 0, \end{aligned} \quad (7.5)$$

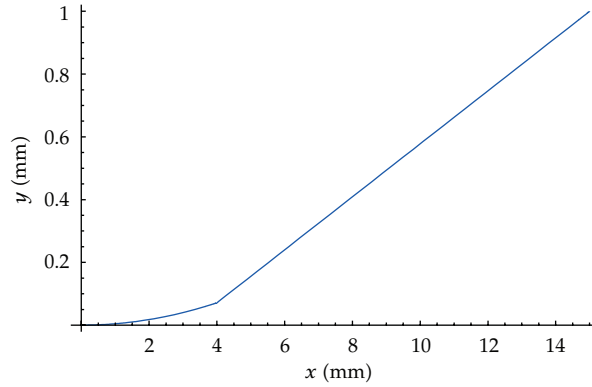


Figure 8: Example of a rotational curve of a parabolic-conic bimetallic shell.

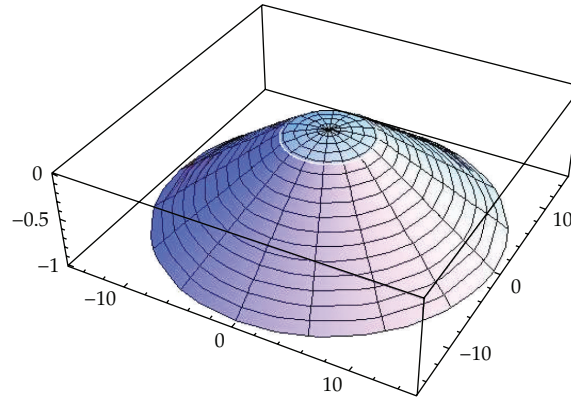


Figure 9: Example of the full shape of a parabolic-conic bimetallic shell.

and the equation for the equilibrium of forces becomes

$$2k^2x^3\mu - u + xu' + x^2u'' = 10k^2x^3, \quad (7.6)$$

with the solution with respect to displacement u

$$u(x) = \frac{kx(8(\alpha_1 + \alpha_2)\delta + 3a^2k(\alpha_1 - \alpha_2)(\mu - 1) - 3kx^2(\alpha_1 - \alpha_2)(5 + \mu))}{12(\alpha_1 - \alpha_2)}, \quad (7.7)$$

that at the same time also satisfies the boundary condition (6.16) at the point $x = a$ and the boundary condition (6.20) for the displacement u at the point $x = 0$. Therefore, at the temperature $T = T_m$ the parabolic shell is completely flattened. The reader should also note that such a state of the shell is only stable with shells that are shallow enough!

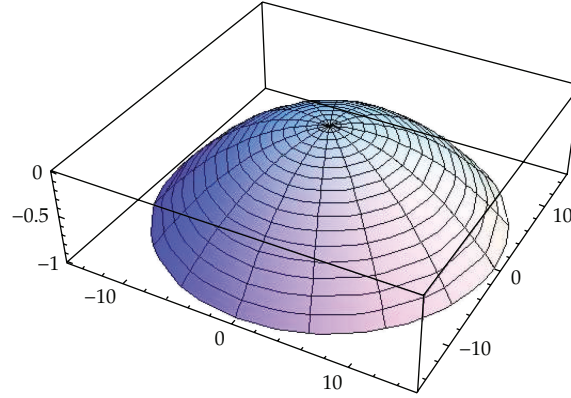


Figure 10: Initial shape of the parabolic shell.

7.2. Numeric Solution of the BVP

We solved the system of (6.21) using the nonlinear shooting method. First, the BVP (6.21) was converted into the system of ordinary differential equations of the first order

$$\begin{aligned}
 y_1' &= y_2 & y_3' &= y_4 & y_4' &= y_5, \\
 y_2' &= \frac{1}{2x^2} \left(2y_1 - 2xy_2 - xy_4^2 - 2x^2y_4y_5 + xy_4^3\mu + 2y_3y_4' - 2xy_4\mu y_4' - 2xy_3y_4'' - 2x^2y_4y_4'' \right. \\
 &\quad \left. - 2x^2y_3y_4''' \right), \\
 y_5' &= \frac{1}{2Bx^2} \left(2cx + 2By_4 - 2PTx^2y_4 + 2Ax^2y_2y_4 + Ax^2y_4^3 - 2Bxy_5 \right. \\
 &\quad \left. + 2Axy_1y_4\mu - 2x \int_0^x xpdx - 2Axy_3\mu y_4'^2 + 2Ax^2y_3y_4y_4'' \right. \\
 &\quad \left. + xy_4' \left(2PTx - A \left(2xy_2 + xy_4^2 + 2y_1\mu - 2y_3y_4\mu \right) - 2Axy_3y_4'' \right) \right) \\
 y_1(0) &= 0, & y_3(0) &= 0, & y_4(0) &= 0, \\
 PT &= A \left(y_2 + \frac{1}{2}(y_4)^2 + \frac{\mu(y_1 + y_3y_4')}{x} + y_3y_4'' \right) \Big|_{x=a}, & QT &= \left(\frac{B\mu y_4}{x} + By_5 \right) \Big|_{x=a},
 \end{aligned} \tag{7.8}$$

when the substitution is introduced

$$u(x) = y_1, \quad u'(x) = y_2, \quad w(x) = y_3, \quad w'(x) = y_4, \quad w''(x) = y_5. \tag{7.9}$$

We chose the approximate values for $y_2(0)$ and $y_5(0)$ and calculated the approximate values for the displacements u and w by the classic one-step fourth-order Runge-Kutta method [23]. Defining more exact values for $y_2(0)$ and $y_5(0)$ was carried out by the Newton method [24]

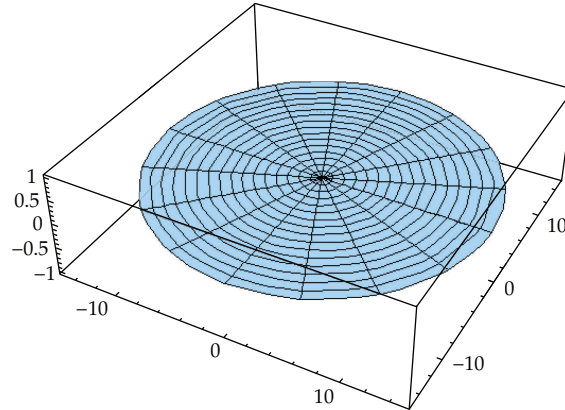


Figure 11: Deformation of the parabolic shell at the temperature $T = T_{mp} = 88.9^\circ\text{C}$ into a regular circular plate shape.

for solving nonlinear equations. We wrote the shell deformation with the ratio ξ between the current height h of the deformed shell and the initial height h_0 of the undeformed shell

$$\xi = \frac{h}{h_0} = \frac{y(a) - w(a)}{y(a)}. \quad (7.10)$$

The program code was written in Mathematica package 7.01.0.

As the components u and w of the displacement vector \vec{u} at the temperature T_m for a totally flattened parabolic shell are defined by (7.3) and (7.7), it is possible to calculate how much the numeric results differ from the actual ones. In this manner, we can estimate the accuracy of the chosen numeric method.

7.3. Temperature Loading of a Parabolic Shell

Let us first observe the stability conditions at temperature loading of a parabolic bimetallic shell with $b = a$ in (7.1). For this special example of a parabolic-conic shell, we calculated, with the earlier mentioned method, the stability conditions at temperature loading. The obtained results are identical to the results calculated by Wittrick et al. [3] for the parabolic shell.

Figure 12 shows stability conditions for a parabolic shell with the material and geometric properties in (7.2). The graph of the function of dimensionless temperature $\tau = T/T_m$ depending on the ratio of heights ξ represents the stability circumstances during the shell's temperature load.

During the initial state of no temperature load $\tau = 0$, at point $O(1,0)$, the ratio of heights is equal to one. By increasing the dimensionless temperature τ , this ratio decreases. As is clear in Figure 12, the segment on the curve between the point O and the point $A(\xi_u, \tau_u) = A(0.44, 1.51)$, where the function $\tau(\xi)$ has a local maximum, is the region of stable equilibrium. The upper snap-through of the shell will, therefore, occur at point A at the temperature of $\tau_u = 1.51$, because the segment between the points A and $C(\xi_l, \tau_l) = C(-0.44, 0.49)$, where the function has a local minimum, is the region of unstable equilibrium.

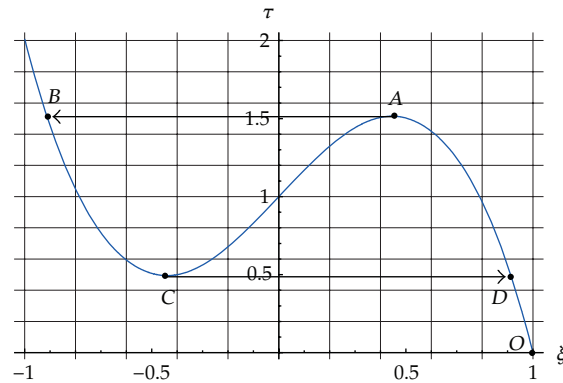


Figure 12: The function $\tau = \tau(\xi)$ as an example of parabolic axisymmetric shell expressing the phenomenon of a system snap-through between points AB in the process of heating up and the points CD in the process of cooling.

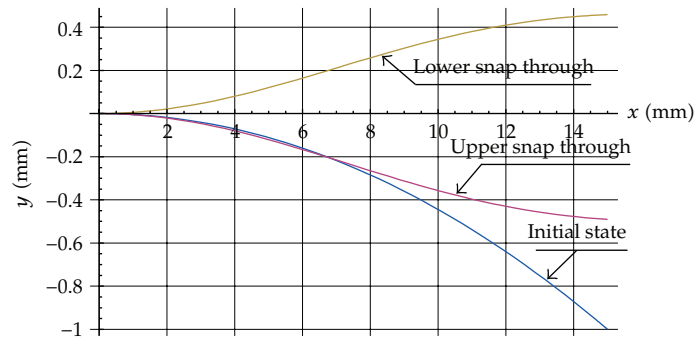


Figure 13: Rotational curves for an undeformed parabolic shell at the moment of the upper and lower snap-through.

After the snap-through, the shell will occupy a new position of stable equilibrium in point $B(-0.91, 1.51)$ at the temperature $\tau = 1, 51$. With further heating of the shell, the ratio ξ continues to decrease.

During the cooling of the shell, we have the opposite phenomenon and at point C at the temperature $\tau_l = 0.49$ another lower snap-through. This time the shell snaps-through into the stable equilibrium position at point $D(0.91, 0.49)$ at the temperature $\tau = 0.49$. By reheating the shell to the temperature of the upper snap-through $\tau_u = 1.51$, we can repeat the complete cycle of the snap-through of the shell. The shape of the shell in the characteristic stages of temperature loading is clear in Figures 13 and 14.

From Figure 12, it follows that in a flattened state at the ratio of heights $\xi = 0$, the shell cannot endure as the point $(0, 1)$ belongs in unstable region between the points A and C . Equation (7.4) determines the temperature T_m at which the shell flattens, Figure 11. If at the temperature $T = T_m$ the flattened shell deflects downwards so that the ratio of heights is $\xi < 0$, then the temperature T_m of the shell is too high for an equilibrium state of the shell at the ratio of heights $\xi < 0$. The apex of the shell accelerates downwards so that a new stable

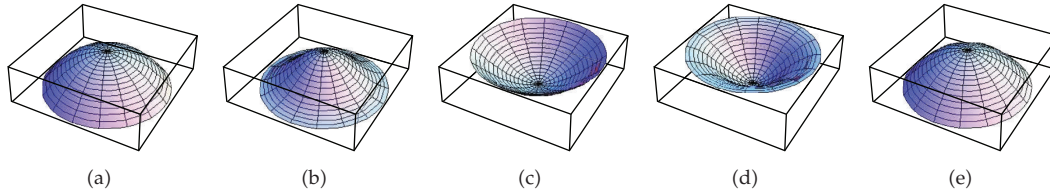


Figure 14: Geometry of a parabolic shell: (a) undeformed, (b) at the upper snap-through, (c) after the upper snap-through, (d) at the lower snap-through, and (e) after the lower snap-through.

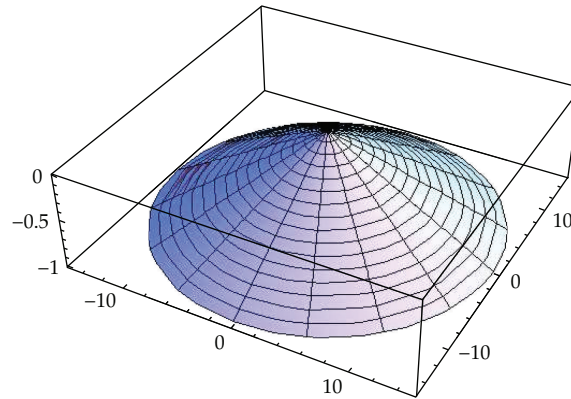


Figure 15: Initial shape of the conic shell.

equilibrium state is established in the position $(-0.78, 1)$. It is quite similar if the shell deflects upwards $\xi > 0$ except that in this case, the temperature $T = T_m$ for the ratio of heights $\xi > 0$ is too low to satisfy the conditions for equilibrium and consequently the apex of the shell accelerates upwards so that the new stable equilibrium state is established in the position $(0.78, 1)$, Figure 12.

7.4. Temperature Loading of a Conic Shell

If in (7.1) $b = 0$, then the shell translates into a conic shape, Figure 15. We present an example of a temperature loaded conic shell with material and geometric properties in (7.2) and a rotational curve $y(x)$

$$y(x) = kx = \frac{1}{15 \text{ mm}}x. \quad (7.11)$$

In comparison with the earlier described parabolic shell, the conic shell has a snap-through at a lower temperature. The upper snap-through occurs at temperature $\tau = 1.00$ and at the height ratio $\xi = 0.41$, Figure 16(b). The shape of the shell after the snap-through is in Figure 16(c). The repeated (lower) snap-through occurs at temperature $\tau = 0.98$ and at the

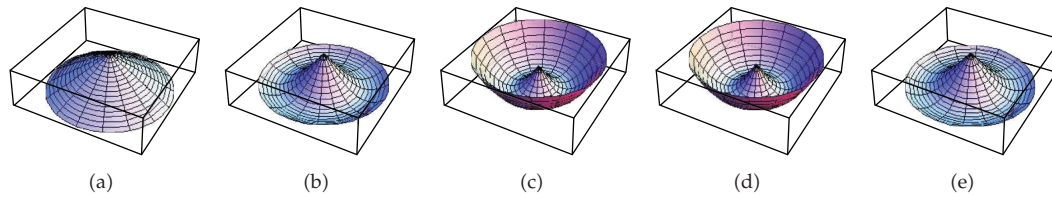


Figure 16: Geometry of a conic shell: (a) undeformed, (b) at the upper snap-through, (c) after the upper snap-through, (d) at the lower snap-through, and (e) after the lower snap-through.

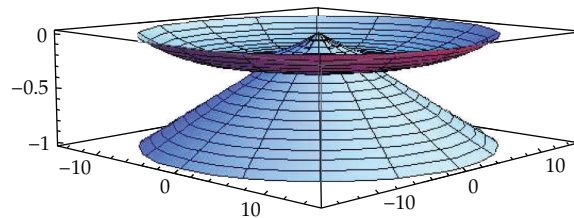


Figure 17: The initial and deformed conic shell at the ratio of heights $\xi = 1$ and $\xi = 0$.

height ratio $\xi = -0.09$, Figure 16(d). The shell snaps-through into a new stable equilibrium position and assumes the shape on the diagram, Figure 16(e).

We would expect, like in the case of a flattened parabolic shell, Figure 11, that at a certain temperature the conic shell would also flatten with the function $y(x) = kx$. It is verified that it is not possible to identically satisfy (6.12) with the displacement $w(x) = y(x) = kx$, thus a flattened state of a conic bimetallic shell is not possible. The shape of the deformed conic shell at the ratio of heights $\xi = 0$ is shown in Figure 17.

7.5. Temperature Loading of a Parabolic-Conic Shell

We gradually increased the value of the parameter b in the equation system (6.21) and calculated the temperature of both snap-throughs for a parabolic-conic type bimetallic shell. The snap-through temperatures T_u and T_l at the parameter b values between $0 \leq b \leq a$ are shown in Table 1.

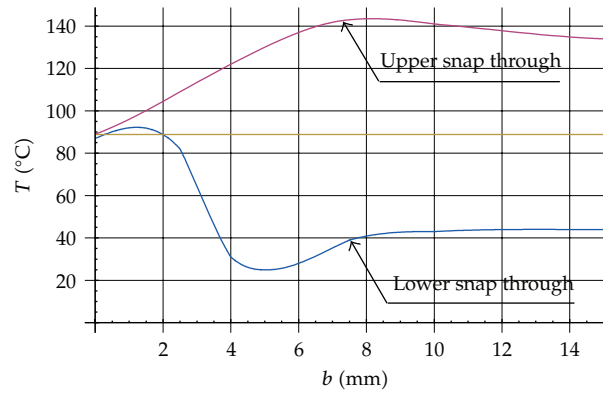
We ascertained that the snap-through temperature is dependent from point b , where the parabolic rotational curve translates into a conic one, Figure 18.

Figure 18 shows how both snap-through temperatures are relative to parameter b . At the extreme point on the left at $b = 0$, an example of the conic shell is shown, and on the right at $b = 15$, an example of parabolic shell is shown.

Both curves for the snap-through temperature have a local extreme. The highest temperature at which the shell snaps-through for the first time (upper snap-through) is $T_u = 143^\circ\text{C}$ at $b = 8.1$ mm. The lowest temperature of the return (lower) snap-through is 25°C at $b = 5.0$ mm. The difference in the temperature of the upper and lower snap-through relevant to the parameter b is evident in Figure 19.

Table 1: Snap-through temperatures of a parabolic-conic shell relevant to the parameter b .

b (mm)	0	1	2.5	4	5	6	7.5	10	12.5	15
T_u (C°)	89	96	109	122	130	137	143	141	137	134
ξ_u	0.41	0.40	0.38	0.38	0.39	0.40	0.43	0.49	0.47	0.49
T_l (C°)	87	92	82	31	25	28	39	43	44	44
ξ_l	-0.09	-0.21	-0.54	-0.59	-0.60	-0.57	-0.49	-0.49	-0.5	0.48

**Figure 18:** Snap-through temperatures of a parabolic-conic type of bimetallic shell.

7.6. Temperature and Force Loading of a Circular Plane-Parabolic Shell

In practice, a shell composed of a circular plane near the apex and a parabola at the edge is frequent, Figure 20. Such a shell occurs with the curve rotation:

$$y(x) = \begin{cases} 0, & x \leq b, \\ \frac{1}{(a^2 - b^2)}x^2 + \frac{b^2}{b^2 - a^2}, & x > b. \end{cases} \quad (7.12)$$

We will again numerically discuss the example of a shell with material and geometric properties in (7.2). The parameter b where the shell translates from a plane into a parabola should have a value of $b = 7.5$ mm. At first, the shell should be loaded only with temperature T . The upper snap-through of such a shell occurs at the temperature $T = 180^\circ\text{C}$ and the height ratio of $\xi = 0.48$, Figure 21.

In comparison with a parabolic shell of equal material and geometric properties, Figure 10, this shell has a snap-through at a much higher temperature. A parabolic shell already translates into an unstable equilibrium state at the temperature $T_u = \tau_u T_m = 134^\circ\text{C}$, when it snaps-through into a new stable equilibrium position. Therefore, with an equal initial height h_0 , the combined shell has a higher temperature of the upper snap-through by 46°C or by 34%. Consequently, with an appropriate combination of a circular plate and parabola it is possible to construct a shell with a low initial height that, despite this, will still have a snap-through at a high temperature. Therefore, this is an important advantage of combined shells in comparison with parabolic shells.

The effect of the concentrated force $F[N]$, exerted at the apex of the shell is clear from Figures 22 and 23. Due to the force, the shell already bends, even when not loaded with

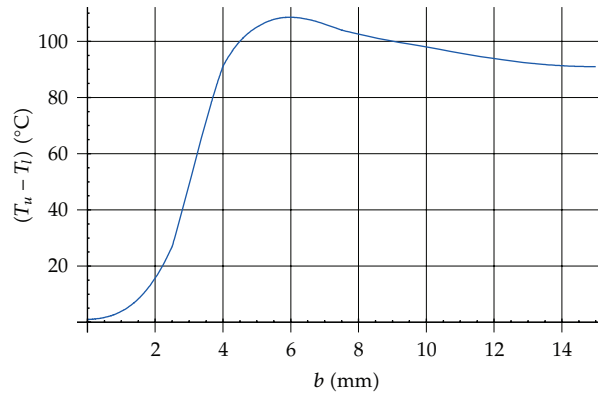


Figure 19: The difference in the temperature of the upper and lower snap-through relevant to the parameter b .

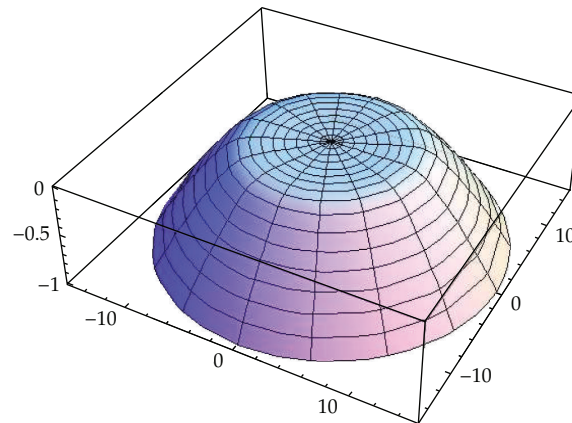


Figure 20: Undeformed shape of a plane-parabola type bimetallic shell.

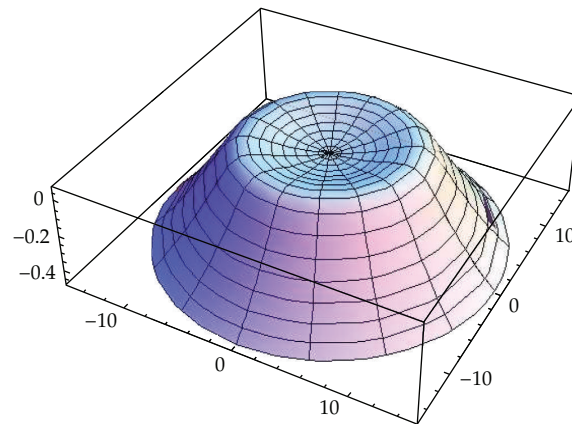


Figure 21: A plane-parabola type bimetallic shell at the moment of the upper snap-through at the temperature $T = 180^{\circ}\text{C}$ and height ratio $\xi = 0.48$.

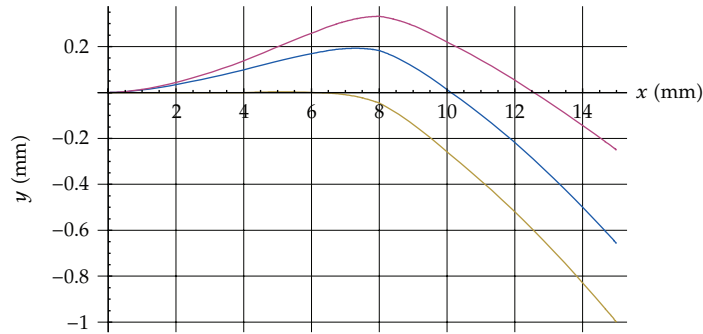


Figure 22: Deformation curve for a plane-parabola type bimetallic shell loaded with a concentrated force $F = 37.7$ N.

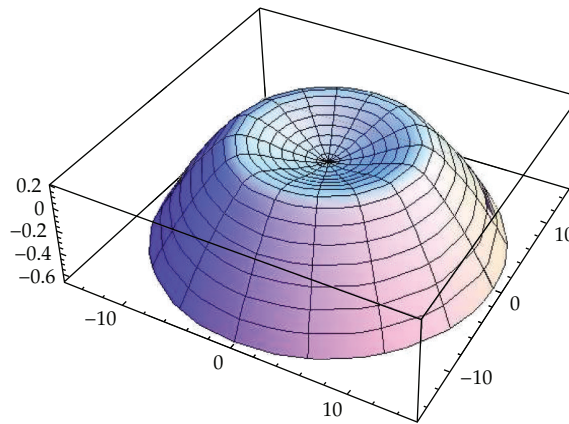


Figure 23: The shape of the shell after loading with a concentrated force $F = 37.7$ N.

temperature, into the shape shown in Figure 23. The concavity is most distinct near the apex. The deformation curve is shown in Figure 22 in blue.

If such a shell is to snap-through it should be additionally heated a bit. The instability and snap-through occurs at temperature $T_u = 65^\circ\text{C}$. The shape of the shell at the moment of snap-through is shown in Figure 24, its deformation curve is shown in Figure 22 in red.

8. Conclusion

Simply supported, thin-walled, shallow bimetallic shells of mixed (combined) type have the property to snap-through at a certain temperature into a new equilibrium position. The temperature of the snap-through depends on the material and geometric properties of the shell. As a special example, we analysed the conditions for parabolic, conic, parabolic-conic and plate-parabolic type of shell that have both layers equally thick $\delta_1 = \delta_2 = \delta/2$, and the same Poisson's ratio $\mu_1 = \mu_2 = \mu$. Two parabolic shells of different rotational curves $y_1 = k_1x^2$ and $y_2 = k_2x^2$ have at the same temperature load T equal relative displacements

$$\frac{u_1}{a_1} = \frac{u_2}{a_2}, \quad \frac{w_1}{a_1} = \frac{w_2}{a_2}. \quad (8.1)$$

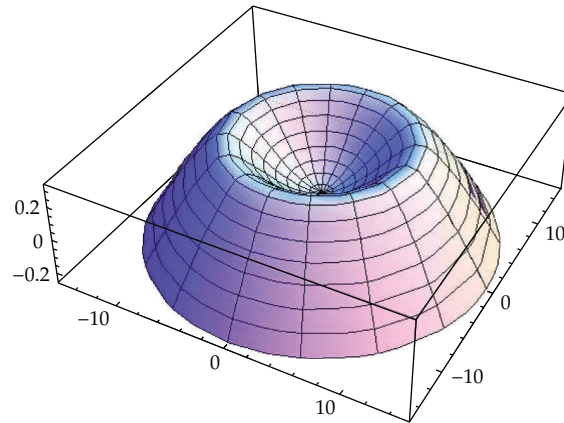


Figure 24: The shape of the shell at the moment of the upper snap-through when loaded with a force $F = 37.7$ N and temperature $T_u = 65^\circ\text{C}$.

If

$$k_1 a_1 = k_2 a_2, \quad \frac{\delta_1}{a_1} = \frac{\delta_2}{a_2}. \quad (8.2)$$

Conic shells with different functions of rotational curves $y_1 = k_1 x$ and $y_2 = k_2 x$ have equal relative displacements (8.1) if the geometry parameters are such that

$$k_1 = k_2, \quad \frac{\delta_1}{a_1} = \frac{\delta_2}{a_2}. \quad (8.3)$$

A conic shell in comparison with a parabolic shell with equal material and geometric properties snaps-through at lower temperatures, Table 1. With a suitable initial shape of a parabolic-conic type bimetallic shell, we can change the upper T_u and lower T_l temperature values at which snap-through occurs. By reducing the conic part of the shell at the expense of the parabolic, the temperature of the upper snap-through increases. It is possible to achieve the highest snap-through temperature T_u if the shell translates from a conic shape to a parabolic approximately at the middle of the horizontal radius a . Therefore, for this type of shell, it is possible to influence the upper and lower temperature snap-through by changing the parameter b , and consequently with it the temperature at which a device would at first shutdown, then after cooling sufficiently start up again. We have ascertained a similar property of changing the temperature of both snap-throughs in parabolic shells with a circular opening in the apex [9]. It is also possible to influence the snap-through temperature by changing the force at the apex of the shell. At a certain force, the shell can snap-through without heating.

References

- [1] S. P. Timoshenko and J. M. Gere, *Theory of Elastic Stability*, McGraw-Hill, New York, NY, USA, 1961.
- [2] D. V. C. Panov, "Prikladnaja matematika i mehanika," *Journal of Applied Mathematics and Mechanics*, vol. 11, pp. 603–610, 1947 (Russian).

- [3] W. H. Wittrick, W. H. Wittrick, D. M. Myers, and W. R. Blunden, "Stability of a bimetallic disk," *Quarterly Journal of Mechanics and Applied Mathematics*, vol. 6, no. 1, pp. 15–31, 1953.
- [4] H. B. Keller and E. L. Reiss, "Spherical cap snapping," *Journal of the Aero/Space Sciences*, vol. 26, pp. 643–652, 1959.
- [5] M. Vasudevan and W. Johnson, "On multi-metal thermostats," *Applied Scientific Research, Section B*, vol. 9, no. 6, pp. 420–430, 1963.
- [6] B. D. Aggarwala and E. Saibel, "Thermal stability of bimetallic shallow spherical shells," *International Journal of Non-Linear Mechanics*, vol. 5, no. 1, pp. 49–62, 1970.
- [7] L. Ren-Huai, "Non-linear thermal stability of bimetallic shallow shells of revolution," *International Journal of Non-Linear Mechanics*, vol. 18, no. 5, pp. 409–429, 1983.
- [8] G. W. Brodland and H. Cohen, "Deflection and snapping of spherical caps," *International Journal of Solids and Structures*, vol. 23, no. 10, pp. 1341–1356, 1987.
- [9] F. Kosel, M. Jakomin, M. Batista, and T. Kosel, "Snap-through of the system of open shallow axisymmetric bimetallic shell by non-linear theory," *Thin-Walled Structures*, vol. 44, no. 2, pp. 170–183, 2006.
- [10] F. Kosel and M. Jakomin, "Snap-through of the axisymmetric bimetallic shell," in *Proceedings of the 3rd International Conference on Structural Engineering, Mechanics and Computation*, Cape Town, South Africa, September 2007.
- [11] M. Batista and F. Kosel, "Thermoelastic stability of bimetallic shallow shells of revolution," *International Journal of Solids and Structures*, vol. 44, no. 2, pp. 447–464, 2007.
- [12] M. Batista and F. Kosel, "Thermoelastic stability of a double-layered spherical shell," *International Journal of Non-Linear Mechanics*, vol. 41, no. 9, pp. 1024–1035, 2006.
- [13] M. Jakomin, F. Kosel, and T. Kosel, "Thin double curved shallow bimetallic shell of translation in a homogenous temperature field by non-linear theory," *Thin-Walled Structures*, vol. 48, no. 3, pp. 243–259, 2010.
- [14] M. Jakomin, F. Kosel, and T. Kosel, "Buckling of a shallow rectangular bimetallic shell subjected to outer loads and temperature and supported at four opposite points," *Advances in Mechanical Engineering*, vol. 2009, Article ID 767648, 17 pages, 2009.
- [15] P. L. Gould, *Analysis of Plates and Shells*, Prentice Hall, Upper Saddle River, NJ, USA, 1999.
- [16] J. N. Reddy, *Theory and Analysis of Elastic Plates*, Taylor & Francis, London, UK, 1999.
- [17] V. Biricikoglu and A. Kalnins, "Large elastic deformations of shells with the inclusion of transverse normal strain," *International Journal of Solids and Structures*, vol. 7, no. 5, pp. 431–444, 1971.
- [18] E. Carrera, "Historical review of Zig-Zag theories for multilayered plates and shells," *Applied Mechanics Reviews*, vol. 56, no. 3, pp. 287–308, 2003.
- [19] U. Icardi and L. Ferrero, "Multilayered shell model with variable representation of displacements across the thickness," *Composites Part B: Engineering*, vol. 42, no. 1, pp. 18–26, 2011.
- [20] M. Shariyat, "Thermal buckling analysis of rectangular composite plates with temperature-dependent properties based on a layerwise theory," *Thin-Walled Structures*, vol. 45, no. 4, pp. 439–452, 2007.
- [21] V. V. Novozhilov, *The Theory of Thin Shells*, P. Noordhoff, Groningen, The Netherlands, 1959.
- [22] A. E. H. Love, *A Treatise on the Mathematical Theory of Elasticity*, Dover, New York, NY, USA, 1944.
- [23] W. H. Press, S. A. Teukolsky, W. T. Vetterling, and B. P. Flannery, *Numerical Recipes*, Cambridge University Press, New York, NY, USA, 3rd edition, 2007.
- [24] D. J. Hoffman, *Numerical Methods for Engineers and Scientists*, McGraw-Hill, New York, NY, USA, 2001.



Hindawi

Submit your manuscripts at
<http://www.hindawi.com>

